

# Classification of interference-fading tolerant $\Phi$ -OTDR signal using optimal peak-seeking and machine learning [Invited]

Yixin Zhang (张益昕)<sup>1</sup>, Tong Zhou (周桐)<sup>1</sup>, Zhewen Ding (丁哲文)<sup>1</sup>, Yanqing Lu (陆延青)<sup>1</sup>, Xuping Zhang (张旭莘)<sup>1\*</sup>, Feng Wang (王峰)<sup>1</sup>, and Ningmu Zou (邹宁睦)<sup>2\*\*</sup>

<sup>1</sup>Key Laboratory of Intelligent Optical Sensing and Manipulation (Nanjing University), Ministry of Education, Nanjing 210093, China

<sup>2</sup>Department of Chemistry and Chemical Biology, Cornell University, Ithaca, NY 14850, USA

\*Corresponding author: [xpzhang@nju.edu.cn](mailto:xpzhang@nju.edu.cn)

\*\*Corresponding author: [nz86@cornell.edu](mailto:nz86@cornell.edu)

Received October 23, 2020 | Accepted January 19, 2021 | Posted Online March 9, 2021

A simple and effective interference-fading tolerant method for phase-sensitive optical time-domain reflectometry ( $\Phi$ -OTDR) using optimal peak-seeking is proposed. This method can reconstruct the vibration signal with high fidelity under the premise of using only an ordinary single-mode sensing fiber without changing the structure of the traditional  $\Phi$ -OTDR system. Based on the data after interference suppression, we applied different machine learning models to recognize the invasive events category. The promising results show potential applications of  $\Phi$ -OTDR equipment and future implementation with machine learning algorithms.

**Keywords:**  $\Phi$ -OTDR; fading suppression; machine learning.

**DOI:** [10.3788/COL202119.030601](https://doi.org/10.3788/COL202119.030601)

## 1. Introduction

Phase-sensitive optical time-domain reflectometry ( $\Phi$ -OTDR), as a rising star of a fully distributed optical fiber sensor (DOFS), has recently attracted significant attention for its merits like fast response, high sensitivity, and multi-point detection capacity<sup>[1]</sup>. The technology has been widely applied in many important fields like intrusion detection<sup>[2]</sup>, structure health monitoring<sup>[3]</sup>, oil and gas pipeline monitoring<sup>[4]</sup>, underwater acoustic and seismic monitoring<sup>[5]</sup>, and more. In order to extract information from  $\Phi$ -OTDR, early research took the amplitude of Rayleigh backscattering (RBS) light as the sensing parameter and obtained the location and frequency information of external disturbance. It is worth noting that the relationship between intensity changes and vibration is nonlinear, and the variation in intensity magnitude could not represent the magnitude of demodulated vibration. In recent years, researchers have shifted their focus to the phase of RBS due to its linearity with vibration<sup>[6]</sup>. Then, the phase-demodulated  $\Phi$ -OTDR system based on heterodyne coherent detection was proposed. With phase extraction and spatial difference processing, the  $\Phi$ -OTDR technique enables us to realize quantitative detection of the vibration.

However, phase-demodulated  $\Phi$ -OTDR based on heterodyne coherent detection unavoidably suffers from interference fading,

which is commonly attributed to the random nature of RBS<sup>[7]</sup>. Fading problems may make the RBS signal from some fiber sections fall into the destructive area, namely the dead zone. When the signal drops into the dead zone, the signal-to-noise ratio (SNR) would be very poor, and we could hardly demodulate the phase<sup>[8]</sup>. Such fading cases may cause high occurrence of false-alarm events, which brings great inconvenience to the in-field application of  $\Phi$ -OTDR<sup>[9]</sup>.

In this paper, we propose an effective and simple method to suppress interference fading for  $\Phi$ -OTDR sensing systems based on heterodyne detection. Since the phase-demodulated result is positively correlated with RBS intensity, we dynamically track the optimal location of RBS intensity in each section of the sensing fiber for reliable demodulated phase. The performance of our method is first verified in laboratory conditions and then tested in the field. The obtained results show that our method can suppress the occurrence probability of fading areas to a large extent and is expected to extend the engineering application realm of the existing phase-OTDR system.

## 2. Methods

The flow chart of the proposed method is shown in Fig. 1. First, we perform band pass filtering on the beat signal to obtain the

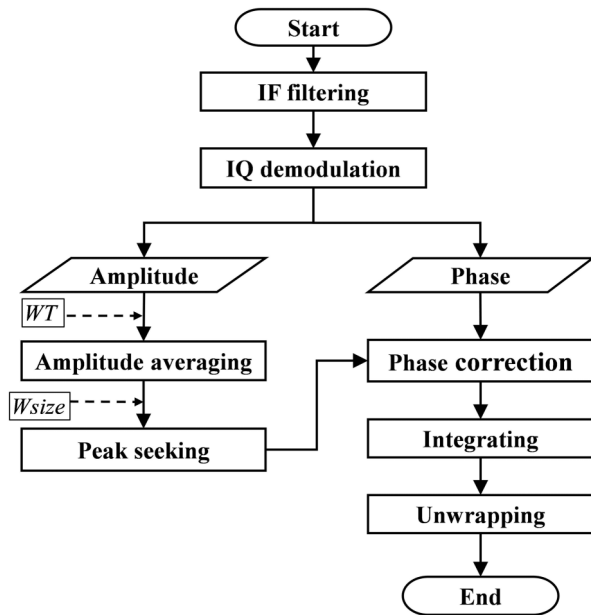


Fig. 1. Flow chart of fading suppression method.

intermediate frequency (IF) component and then perform in-phase quadrature (IQ) demodulation<sup>[10]</sup> to obtain its amplitude and phase. Then, we select the time-domain (TD) amplitude average window and average the amplitude along the time axis. Then, we select the window size  $W_{size}$  and equally divide the amplitude trace into  $N$  intervals along the distance axis to obtain the signal strength value at the same location.  $N$  is the downward integral value of  $n/W_{size}$ , and  $n$  is the number of sampling points. These moving average results were used for selecting the optimal location. However, different  $W_{size}$  will cause the probability density function distribution to change. Figure 2(a) shows the probability of the maximum amplitude falling into the dead zone under different  $W_{size}$  (10 dB SNR guaranteed). Since the probability of falling into the dead zone is also different under different pulse widths, we designed an experiment. Figure 2(b) shows the probability of the maximum amplitude falling into the dead zone under different pulse widths (10 dB SNR guaranteed). According to the statistical results of Fig. 2, the  $W_{size}$  selected should cover at least two spatial resolutions.

Then, the position of amplitude peak in each interval is found, and the phase difference between nearby peaks is calculated. TD differencing is further performed on the phase difference result between current and previous measurements. Then, the vibration applied on the fiber could be reconstructed through integration and unwrapping<sup>[11]</sup>.

Performance of the proposed method is verified by commercial  $\Phi$ -OTDR equipment (Ada-5032E, Nanjing Fiber Technology Co., Ltd.), as shown in Fig. 3(a). Its internal structure and experiment setup are shown in Fig. 3(b).

A 3.7 kHz line-width laser (narrow-linewidth laser, NLL) operating at 1550.12 nm was selected as the light source. The output of the NLL was split into two parts at 80% and 20% as

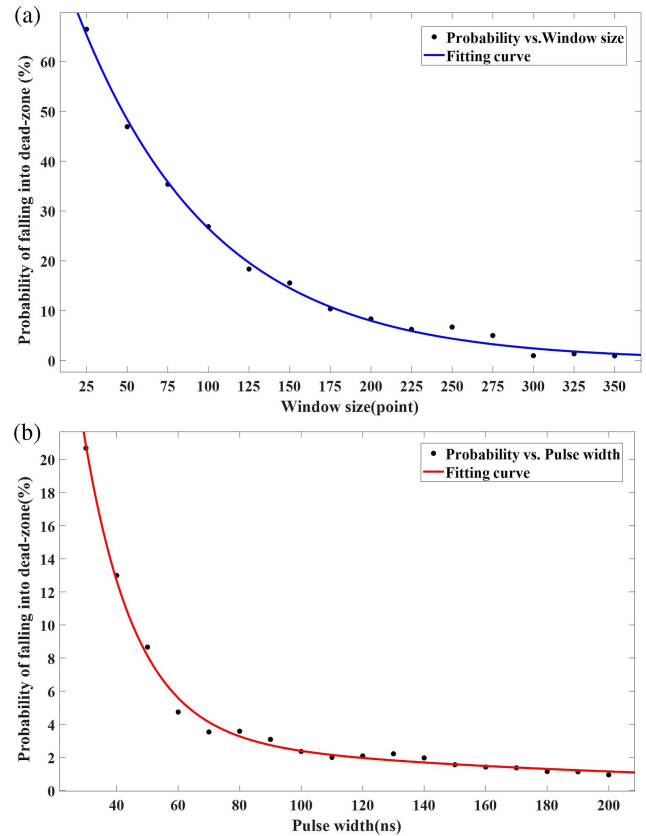


Fig. 2. (a) Probability of signal falling into the dead zone under different window size (100 ns). (b) Probability of signal falling into the dead zone under different pulse width.

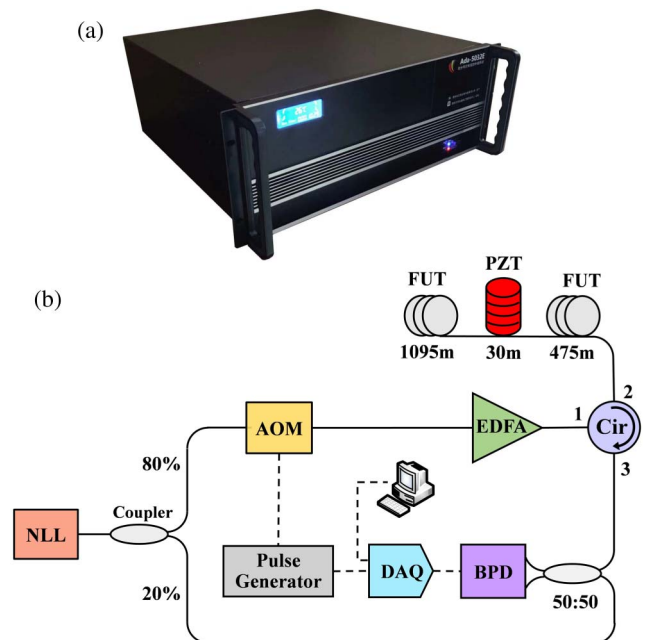


Fig. 3. (a) Ada-5032E. (b) Schematic diagram of the experiment. (NLL, narrow-linewidth laser; AOM, acoustic-optical modulator; FUT, fiber under test; EDFA, erbium-doped fiber amplifier; Cir, circulator; BPD, balanced photodetector; DAQ, data acquisition card; PZT, piezo transducer.)

the probe light and the local reference light, respectively, by an optical coupler. The probe part was modulated into probe pulse with 150 MHz frequency shift induced by an acoustic-optic modulator (AOM). The probe pulse with pulse width of 100 ns and repetition rate of 1 kHz was amplified in an erbium-doped fiber amplifier (EDFA) and then launched into the fiber under test (FUT) through a circulator.

To simulate the external vibration, a piezo transducer (PZT) wrapped with 30-m-long single-mode fiber was located around 475 m along the sensing fiber, which is driven by a sinusoidal voltage signal with the frequency of 25 Hz. Then, a 1095 m fiber was placed at the far end of the FUT. The RBS light returning from the FUT mixed with the local reference light and finally was detected by a balanced photo detector (BPD) with 200 MHz bandwidth. An 8 bit data acquisition card (DAQ) continuously sampled the output data with a 1 GHz sampling rate. The phase demodulation was completed on a personal computer. We continuously recorded data for 300 s to guarantee that the RBS signal from all regions has enough time to experience various possible states. We take the 15 s phase result to show and perform short-time Fourier transform (STFT) to it. It can be clearly seen from Fig. 4 that the phase results obtained by the traditional method have eight errors in 4–9 s and 11–14 s, while the phase results obtained by the proposed method have no errors in 15 s.

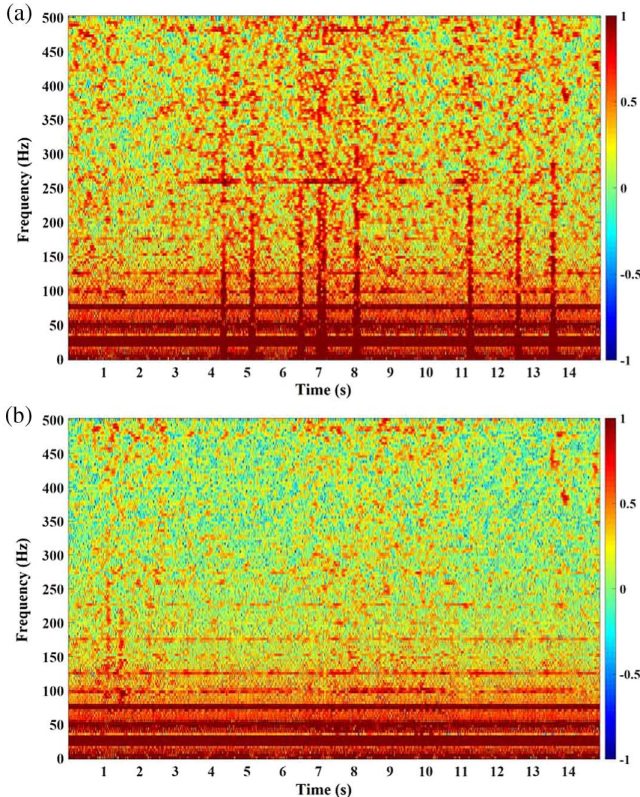


Fig. 4. STFT spectrum of phase results in 15 s. (a) Traditional method. (b) Proposed method.

### 3. Results

The phase results obtained by the proposed method within 5 min were statistically analyzed and compared with the traditional method. As shown in Fig. 5, the accuracy of the proposed method is always superior to the traditional method. To further verify the feasibility of our proposed method, we made an in-field test of buried power cable anti-breakage monitoring using a  $\Phi$ -OTDR running both the traditional and proposed algorithms. We hit the ground 15 m away from the cable 10 times with periods around 3 s. Figure 6 shows the STFT spectrum of

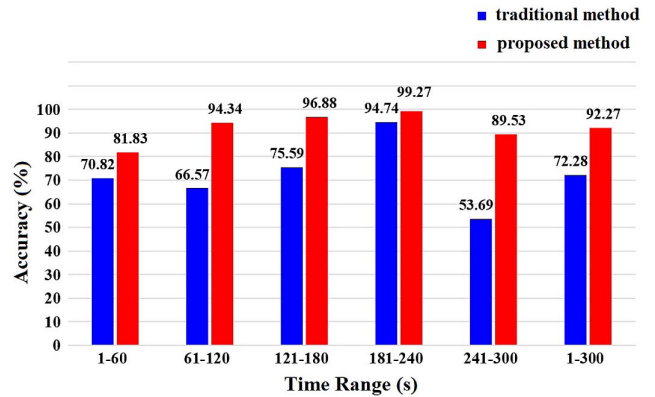


Fig. 5. Accuracy of two methods within 5 min.

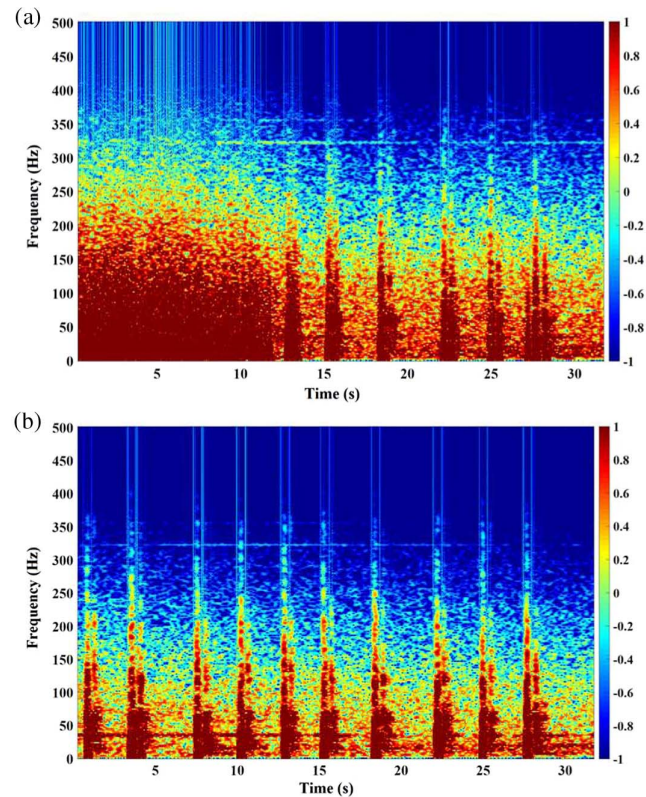


Fig. 6. STFT spectrum of 10 ramming ground tests. (a) Traditional method. (b) Proposed method.



the events. Obviously, we can clearly distinguish 10 ramming with the proposed method, while the first four events were submerged in the noise if the traditional method is applied. Our fading suppression did lower the location accuracy as a tradeoff of the wider range of detectable frequency. In our experiment, the original instrument setup can tell the invasive events within  $\pm 10$  m, and the processed data can tell events located within  $\pm 20$  m. We are able to tell if the signal is a false alarm and further differentiate the type of invasive events through machine learning algorithms in real applications. This ability is much more important than the  $\pm 10$  m location accuracy. Furthermore, we are still able to detect the event locations by backtracking signals from neighboring regions and doing further analysis based on their phase and strength data separately.

Based on different applications, triggering events would have varied features and characteristics. In this research, we are focusing on events that could damage the infrastructure constructions, such as the invasive events of electric power transmission lines and tunnel construction accidents. In these physically invasive events, we need to recognize and differentiate disturbing cases, which may contain digging, knocking, hammering, and so on. It is computationally expensive to deal with original events data without data processing and filtering. Therefore, it is necessary to extract and digitalize event characteristics and reduce background noise so that both the training and testing models can be applied to events effectively (Table 1). We used multiple feature extraction algorithms based on the TD and frequency-domain (FD) signals from the invasive events. For the TD feature extraction, we first calculated the signal energy (SE) as

$$SE = \sum_{i=0}^{n-1} |x(n)|^2. \quad (1)$$

Because SE is sensitive to high levels, if a sampling point has serious distortion, it will have a great impact on the parameters. Our proposed method has a good effect on signal distortion so that events with outlier SE can be removed. We also take the mean amplitude and standard deviation of all events into consideration. Moreover, the disturbance duration of the signal can reflect whether the disturbance event is transient or long-term. So, we divide duration  $t$  into three levels, which will also be used to distinguish events:

$$L(t) = \begin{cases} 1 \text{ (short)}, & 0 < t < 5 \text{ s} \\ 2 \text{ (medium)}, & 5 < t < 30 \text{ s} \\ 3 \text{ (long)}, & t > 30 \text{ s} \end{cases} \quad (2)$$

To better extract the FD features, we first process the data with STFT. We observed an example of an excavator digging event, as shown in Fig. 7.

Based on the characters of events we collected, we categorized all events into five different types; each of them was labeled as 1–5 (Table 2). Then, we extracted all TD features of these events, such as SE, signal variance, and  $L(t)$ . After STFT transfer, we set

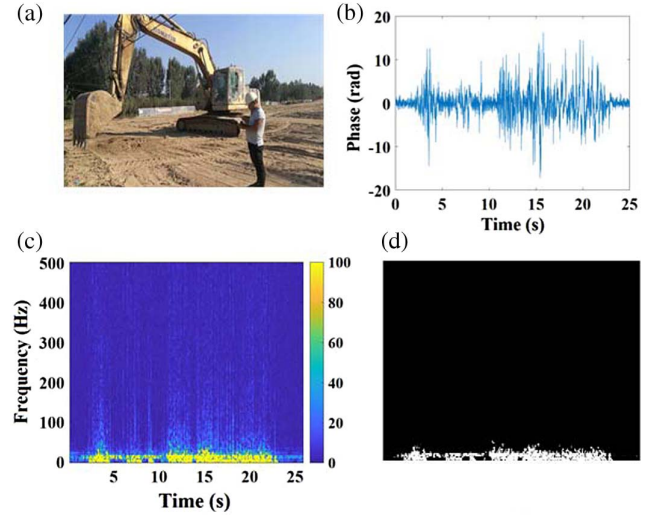


Fig. 7. (a) Excavator digging event. (b) Time domain wave pattern of an invasive event. (c) Frequency-domain image after STFT. (d) Binary image after threshold filtering.

a pixel value threshold and changed the original pattern into a binary image. Then, we extracted nine features from both TD and FD patterns. We applied the support vector machine (SVM)<sup>[12]</sup> and feedforward neural network on the pattern recognition of these signals. Before classification, we randomly selected 283 cases as the training dataset, in which the number of cases in each category is 69:107:40:28:39. The rest of the cases were treated as a testing dataset for the model evaluation. An

Table 1. Definition of Pattern Features.

Feature	Symbol	Description
Area	S	Total number of pixels
Perimeter	P	Number of pixels on edge
Compactness	Con	(Square of P)/S
Number of clusters	Nc	Number of connected pixel clusters

Table 2. Category and Counts of Samples and Labels.

Event Category	Number of Samples	Label
Excavator digging	93	1
Engineering truck passing	148	2
Falling rock	53	3
Pile driver hitting	37	4
Directional drilling	52	5

**Table 3.** Testing Dataset and Results of Both Models.

Event	Number of Samples	Accuracy (%)	
		SVM	FNN
Excavator digging	24	100	100
Truck passing	41	100	100
Rock falling	13	100	100
Stick ramming	9	67	78
Driller punching	13	100	100

### 4. Conclusions

In this report, a simple and effective method was introduced for interference-fading suppression in the  $\Phi$ -OTDR sensing system. The performance of our method has been demonstrated under both laboratory and field conditions. Experimental results have shown that our method can greatly suppress fading and obtain higher quality demodulated signals, which is expected to be a powerful method to enhance the performance of the  $\Phi$ -OTDR system in engineering applications. Based on the data after interference suppression, we applied different machine learning models to recognize the invasive events category. The promising results show potential applications of  $\Phi$ -OTDR equipment and future implementation with machine learning algorithms.

### Acknowledgement

This work was supported by the National Natural Science Foundation of China (Nos. 61627816 and 61975076), the Beijing Natural Science Foundation (No. 4192042), the Key Research and Development Program of Jiangsu Province (No. BE2018047), the Natural Science Foundation of Jiangsu Province (No. BK20180328), and the Key Technology R&D Program of Inner Mongolia Autonomous Region.

### References

1. X. Bao and L. Chen, "Recent progress in distributed fiber optic sensors," *Sensors* **12**, 8601 (2012).
2. J. C. Juarez and H. F. Taylor, "Field test of a distributed fiber-optic intrusion sensor system for long perimeters," *Appl. Opt.* **46**, 1968 (2007).
3. J. M. López-Higuera, L. R. Cobo, A. Q. Incera, and A. Cobo, "Fiber optic sensors in structural health monitoring," *J. Lightwave Technol.* **29**, 587 (2011).
4. Y. Huang, Q. Wang, L. Shi, and Q. Yang, "Underwater gas pipeline leakage source localization by distributed fiber-optic sensing based on particle swarm optimization tuning of the support vector machine," *Appl. Opt.* **55**, 242 (2016).
5. J. P. F. Wooller and R. I. Crickmore, "Fibre optic sensors for seismic intruder detection," *Proc. SPIE* **5855**, 27 (2005).
6. Y. Lu, T. Zhu, L. Chen, and X. Bao, "Distributed vibration sensor based on coherent detection of phase-OTDR," *J. Lightwave Technol.* **28**, 3243 (2010).
7. P. Healey, "Fading in heterodyne OTDR," *Electron. Lett.* **20**, 30 (1984).
8. M. Zabihi, X. Chen, T. Zhou, J. Liu, F. Wang, Y. Zhang, and X. Zhang, "Compensation of optical path difference in heterodyne  $\Phi$ -OTDR systems and SNR enhancement by generating multiple beat signals," *Opt. Express* **27**, 27488 (2019).
9. F. Pang, M. He, H. Liu, X. Mei, J. Tao, T. Zhang, X. Zhang, N. Chen, and T. Wang, "A fading-discrimination method for distributed vibration sensor using coherent detection of  $\Phi$ -OTDR," *IEEE Photon. Technol. Lett.* **28**, 2752 (2016).
10. Z. Wang, L. Zhang, S. Wang, N. Xue, F. Peng, M. Fan, W. Sun, X. Qian, J. Rao, and Y. Rao, "Coherent  $\Phi$ -OTDR based on I/Q demodulation and homodyne detection," *Opt. Express* **24**, 853 (2016).
11. F. Zhu, Y. Zhang, L. Xia, X. Wu, and X. Zhang, "Improved  $\Phi$ -OTDR sensing system for high-precision dynamic strain measurement based on ultra-weak fiber Bragg grating array," *J. Lightwave Technol.* **33**, 4775 (2015).
12. Y. Shi, Y. Wang, L. Wang, L. Zhao, and Z. Fan, "Multi-event classification for  $\Phi$ -OTDR distributed optical fiber sensing system using deep learning and support vector machine," *Optik* **221**, 165373 (2020).

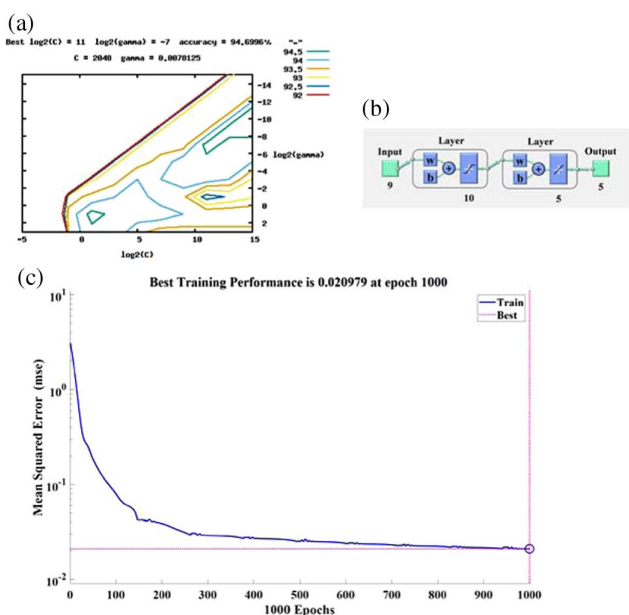


**Fig. 8.** (a) Parameter optimization results of SVM model. (b) Schematic structure of feedforward neural network. (c) Mean squared error.

RBF function was selected as the kernel function when we use an optimized SVM model, in which  $C = 2048$  and  $\gamma = 0.0078$ .

Moreover, we also tried the feedforward neural network for the same training and testing dataset. As shown in Fig. 8(b), there are 10 perceptrons in the hidden layer and five perceptrons in the output layer. We use tansig as the hidden layer transfer function, purelin as the output layer transfer function, and traingdx as the network training function. As a result, both the SVM and neural network models achieve high testing accuracy in most of cases (Table 3). For all cases with labels 1, 2, 3, and 5, both models can achieve 100% accuracy. For cases with the label 4, the accuracy is lower since the pile driver hitting events could be mislabeled as falling rock events (label 3).